Realization of rhombohedral-stacked trilayer graphene by moiré engineering

Ya-Xin Zhao,[1,3] Mo-Han Zhang,[1,3] Zi-Yi Han,[1,3] Ya-Ning Ren,[1,3] Xiao-Feng Zhou,[1,3] Chao Yan,[1,3] Ke Lv,[1,3] Yu Zhang,[2,*] and Lin He[1,3,*]

[1]*Center for Advanced Quantum Studies, Department of Physics, Beijing Normal University, Beijing, 100875, People's Republic of China*
[2]*Advanced Research Institute of Multidisciplinary Sciences, Beijing Institute of Technology, Beijing 100081, People's Republic of China*
[3]*Key Laboratory of Multiscale Spin Physics, Ministry of Education, Beijing, 100875, People's Republic of China*

(Received 19 January 2024; revised 9 April 2024; accepted 16 May 2024; published 29 May 2024)

Rhombohedral (ABC) stacked multilayer graphene hosts low-energy flat bands, which have proven to be an ideal platform toward achieving interaction-driven physics including superconductivity and ferromagnetism. However, of the two common multilayer graphene configurations, ABC stacked graphene is less energy favorable than the Bernal (ABA), as a result, experimental realization of large-area ABC stacked graphene is still big challenge up till now. Here we report a facile method to controllably realize a sub-micrometer-scale ABC stacked trilayer graphene (ABC-TG). By rotating graphene monolayer relative to a bilayer with a tiny angle, we observe a large-area and periodic ABC-TG region after atomic reconstruction. Our experiment indicates that the obtained ABC-TG region is rather stable under thermal annealing and pulse voltages. Using scanning tunneling microcopy (STM), we demonstrate that the flat bands of the ABC-TG region exhibit a pronounced size-dependent characteristic when the size of ABC-TG is smaller than about 100 nm, whereas, the bandwidth of the flat bands becomes a constant when the size is larger than about 100 nm, implying a minimal size for exploring emergent correlated physics in the ABC stacked graphene.

DOI: 10.1103/PhysRevB.109.205155

I. INTRODUCTION

Two-dimensional van der Waals (vdW) materials with an interlayer twist angle θ have proved to be fascinating platforms to realize emergent quantum phase [1–19]. Recent experimental achievements mainly focus on the moiré systems, including twisted bilayer graphene, twisted trilayer graphene, twisted double-bilayer graphene, and twisted transition metal dichalcogenide, all of which host low-energy flat electronic bands at certain twist angle [20–23]. Owing to the quenched kinetic energies, various intriguing correlation-driven ground states, such as correlated insulating states [1,2,5,9], unconventional superconductivity [5–8], ferromagnetism [11–19] and anomalous Hall effects [18], have been observed in one or more of these systems. However, note that the realization of flat bands in twisted graphene materials requires a highly uniform and precise twist angles, which is strongly restricted by the sample fabrication techniques [2,24].

An alternative vdW material for realizing low-energy flat bands is rhombohedral (ABC) stacked multilayer graphene [25–28]. Theoretically, the flat bands of pristine ABC stacked multilayer graphene are right at the Fermi energy with electrical tunability and become sequentially narrower as increasing the layer number [29,30]. Indeed, recent measurements have uncovered the correlated insulating state, superconductivity, and magnetism in the ABC stacked trilayer graphene (hereinafter simply named as ABC-TG) aligned to hexagonal boron nitride (hBN) [31–33]. And shortly afterwards, abundant correlated and topological phenomena have also been reported in ABC stacked tetralayer and pentalayer graphene [25,26,34–40]. These observations establish the ABC stacked multilayer graphene as a promising candidate for exploring emergent physics in flat-band systems.

However, of the two naturally multilayer graphene configurations presented in exfoliated samples, the ABC stacking order is less energy favorable than the Bernal (ABA) [41]. Previous experiments demonstrated that only about 15% of the exfoliated trilayer graphene hosts the ABC stacking order [42]. Moreover, such a fraction of ABC-TG region prefers to transform into the ABA stacking order during a dry-transfer procedure [31,43], which greatly reduces the productivity of the ABC-TG. Chemical vaper deposition (CVD) is another widely used method to synthesize trilayer graphene on metallic substrates [44], where the proportion of the ABC-TG can reach approximately 59%. However, the layer number of CVD-synthesized graphene is usually uncontrollable and heterogeneous. In these regards, it is an urgent need to fabricate large-scale trilayer graphene with a stable ABC stacking order.

In this work, we report a facile method to controllably fabricate stable ABC-TG regions with a submicrometer lateral size. By rotating graphene monolayer relative to a bilayer with an arbitrary tiny angle, we observe a large proportion of periodic ABC-TG regions after atomic reconstruction. Such moiré-confined ABC-TG regions are quite stable and can survive under thermal annealing and pulse voltages. Moreover, our scanning tunneling spectroscopy (STS) measurements further reveal that the bandwidth of the flat bands in the ABC-TG regions becomes a constant and is the same as the bulk phase when the size of the ABC-TG is larger than about 100 nm. Our results highlight a versatile platform for exploring emergent physics in strongly correlated regimes.

*Corresponding authors: yzhang@bit.edu.cn; helin@bnu.edu.cn

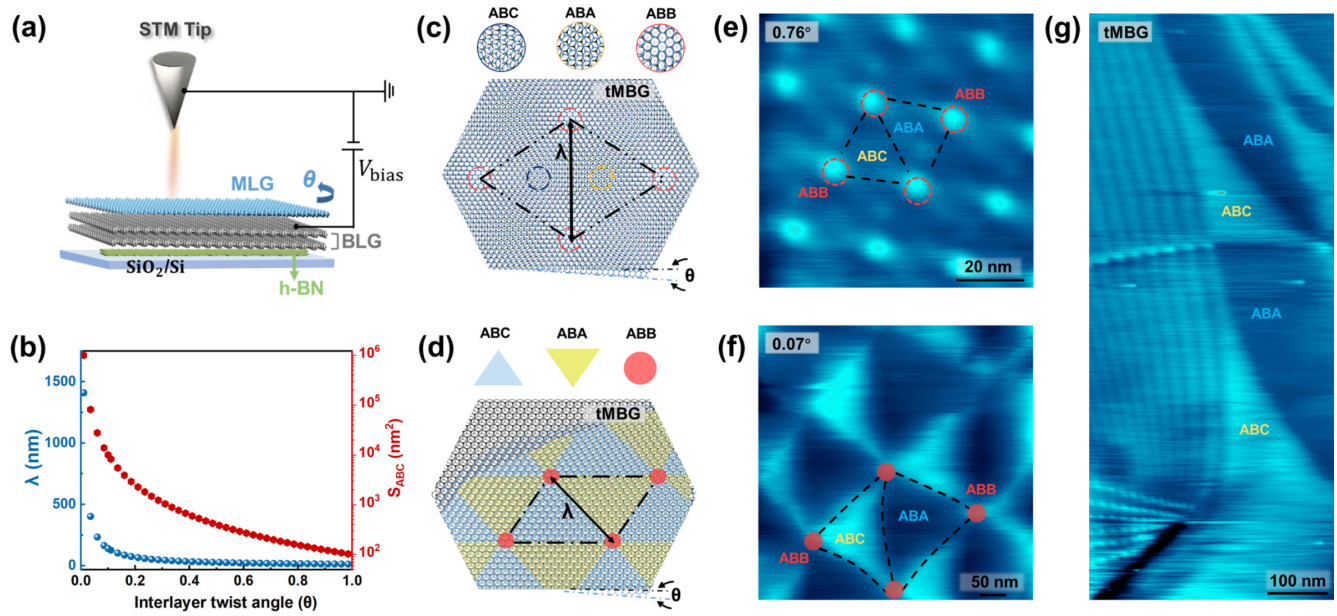

FIG. 1. Atomic insights figure of tMBG. (a) Schematic of the STM set-up on tMBG device. A tMBG is constructed of a monolayer graphene stacking onto a Bernal bilayer graphene with a twist angle θ, and is placed on top of a hBN-covered SiO_2/Si substrate. (b) Relation between interlayer twist angle θ and moiré periodicity λ of the tMBG. (c), (d) Schematics of atomic stacking in tMBG with different twisted angles and the atomic configurations for ABB, ABA, and ABC stacking regions. Atomic reconstruction usually appears at a tiny twist angle. (e), (f) Representative STM images of transfer-assisted tMBG samples with the twisted angle of 0.76° and 0.07°, respectively. The ABB, ABA, and ABC stacked regions are marked in the panels. Scanning parameters: (e) $V_{bias} = 400$ mV, $I = 100$ pA, (f) $V_{bias} = -550$ mV, $I = 200$ pA. (g) Large-scale STM image of a tMBG with the twist angle of about 0.1° under heterogeneous heterostrains.

II. EXPERIMENT

In our experiment, the periodic ABC samples were fabricated by transferring a monolayer graphene onto a Bernal stacked bilayer graphene with a tiny twist angle, labeled as tMBG, via a tear-and-stack method [45–47]. Then, the samples were placed on a hBN-covered SiO_2/Si substrate, as schematically shown in Fig. 1(a) of the STM measurement setup (see Method and Figs. S1–S3 for more details [48]). Similar to the twisted bilayer graphene, the wavelength of moiré pattern λ in the tMBG is determined by the twist angle θ as $\lambda = a/[2\sin(\theta/2)]$, where $a = 0.246$ nm is lattice constant of graphene [see Fig. 1(d)]. For $\theta > 1°$, the atomic registry in the tMBG usually changes continuously across an incommensurate moiré structure, resulting in three distinct stacking orders, i.e., energetically favorable ABA/ABC and unfavorable ABB stacking orders [see Fig. 1(c)]. As decreasing the θ, the interplay between the vdW interaction energy and the elastic energy gradually generates an atomic reconstruction, and finally, resulting in a tessellation of alternating ABA and ABC stacked triangular patterns [49,50], as schematically represented in Fig. 1(d).

III. RESULTS AND DISCUSSION

Scanning tunneling microscopy (STM) topography measurements can be utilized to clearly visualize the atomic reconstruction and precisely identify the stacking orders within the tMBG. Figures 1(e) and 1(f) show typical STM images of our tMBG samples with the twist angles $\theta = 0.76°$ and 0.07°, corresponding to the tMBG without and with the structure reconstruction, respectively. As we can see, the moiré pattern of tMBG without atomic reconstruction ($\theta = 0.76°$) presented in the STM image exhibits bright triangular-arranged ABB stacked regions, which are surrounded by alternative ABA and ABC stacked regions under a smooth evolution [see Fig. 1(e)]. In contrast, for the reconstructed tMBG ($\theta = 0.07°$), the ABB stacked regions are remarkably contracted, and simultaneously, the well-defined ABA and ABC stacked regions equally separate the moiré pattern, showing as dark and bright triangles in the STM contrast (details to distinguish the ABA and ABC stacked regions will be introduced in Fig. 2). Such a STM topography is quite different from that in twisted bilayer graphene, where the AB and BA stacked regions have an identical contrast and are separated by a bright domain wall after the atomic reconstruction [51,52].

Apparently, the area of the ABC-TG region in the tMBG within each supercell (S_{ABC}) is strongly dependent on the interlayer twist angle θ. Especially for a tiny θ, S_{ABC} can be roughly calculated by $100/\theta^2$ nm^2, where a subtle decrease of θ results in a greatly increased S_{ABC}, as plotted in Fig. 1(b). For example, S_{ABC} of the tMBG with $\theta = 0.07°$ given in Fig. 1(f) can be up to 2×10^4 nm^2. Moreover, such a S_{ABC} can be further enlarged under a slight heterostrain, which can be deduced from the distorted moiré patterns in our large-scale STM images shown in Fig. 1(g). It is worth noting that heterostrain is usually inevitable in vdW materials during the sample synthesis and transfer processes [2].Therefore, large-scale ABC-TG regions with a submicrometer lateral size can be successfully achieved in the tMBG. Besides, there is a dense of extremely narrow ABC-TG stripes appearing in strained tMBG, which also provides a

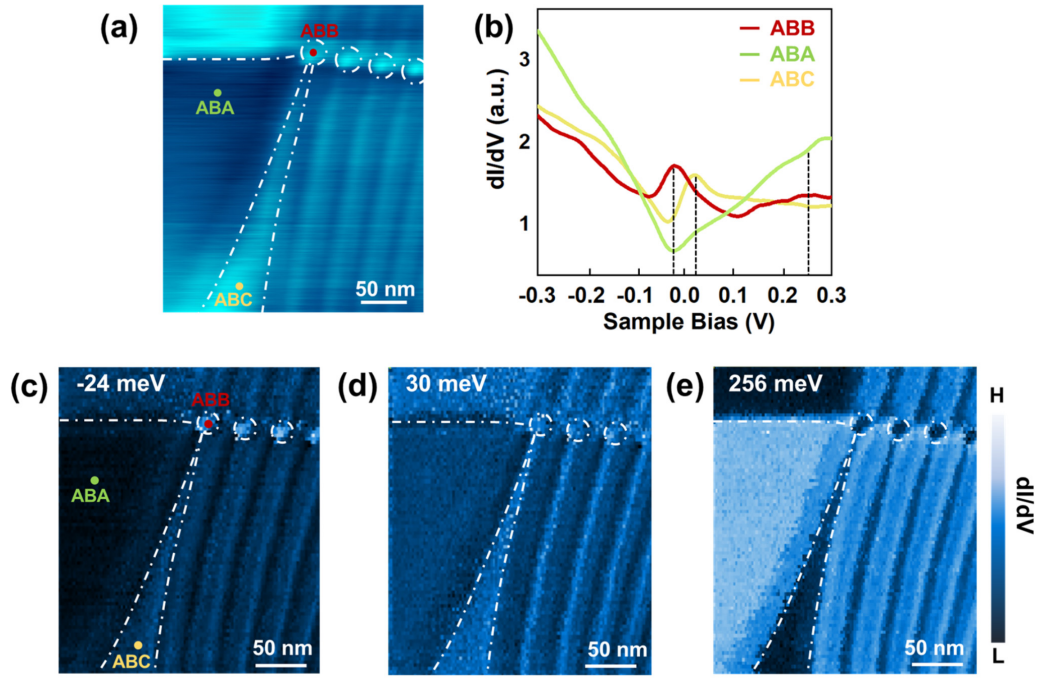

FIG. 2. Electronic properties of tMBG. (a) A typical STM image of a small-angle tMBG under heterogeneous strains ($V_{\text{bias}} = 500$ mV, $I = 100$ pA). (b) Typical STS spectra recorded on ABB, ABA, and ABC stacking regions, respectively. (c)–(f) Corresponding STS maps of the tMBG at the energy of −24, 30, and 256 meV, respectively.

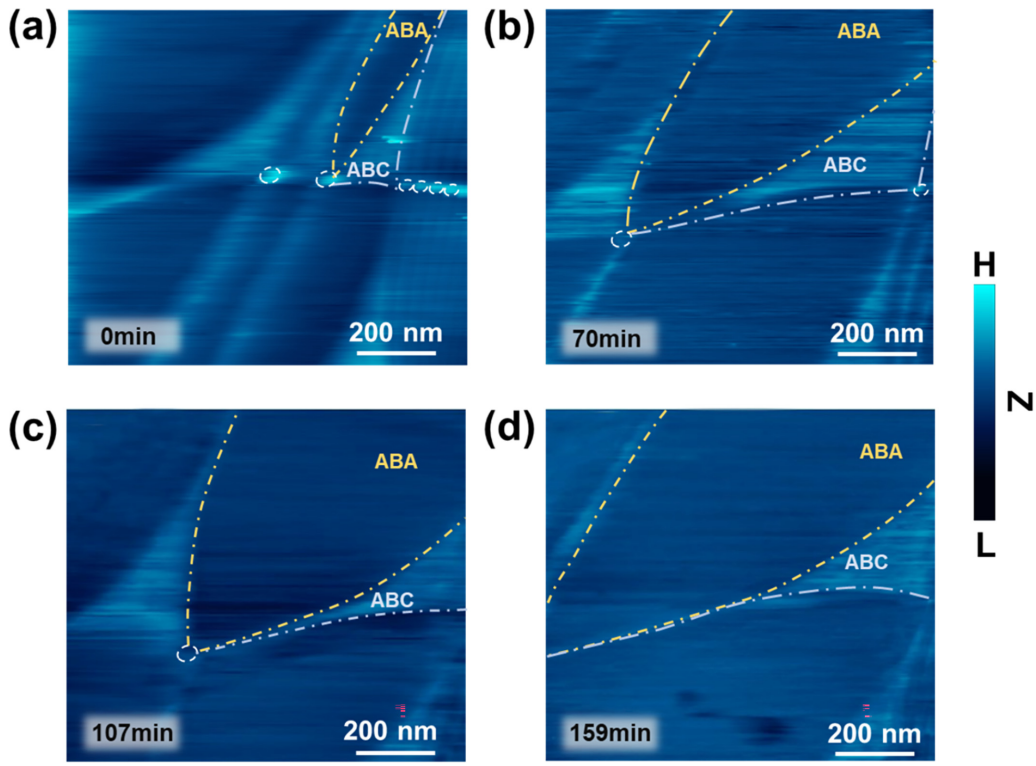

FIG. 3. Tip-manipulated transition of the stacking order in a tMBG. (a) STM topographic image of tMBG with a tiny angle of about 0.1°. The ABA and ABC stacked regions are enclosed by the yellow and gray dotted lines, respectively. (b)–(d) The evolution of the atomic stacking orders after applying a STM tip pulse with the voltage of 6 V for 60 ms. The ABC-TG regions are robust and stable after the structure relaxation.

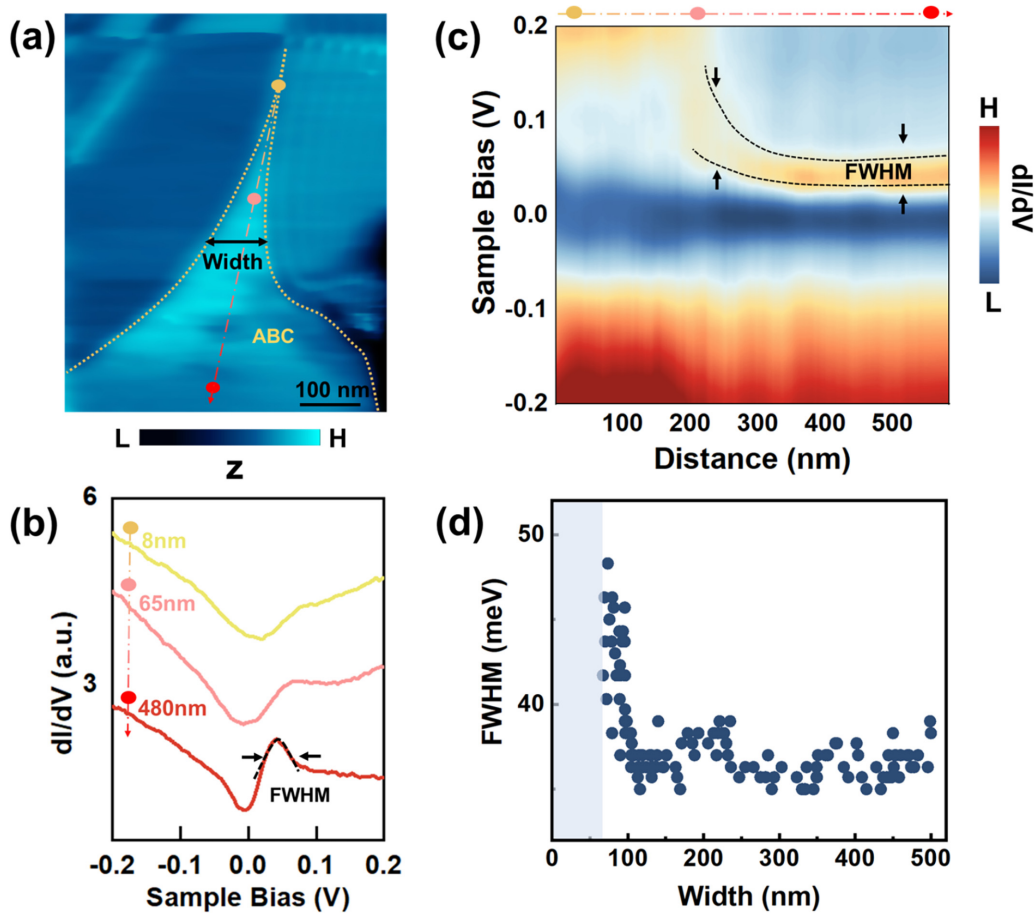

FIG. 4. Electronic properties of finite-size ABC-TG in tMBG. (a) Representative STM image of tMBG with a small twisted angle and a large heterostrain after the atomic reconstruction. The width of the ABC-TG is defined as the lateral length marked by the black double-headed arrow. (b) Typical STS spectra recorded on the locations marked in (a), with the width of 8, 65, and 480 nm, respectively. (c) The evolution of STS spectra recorded along the red arrow marked in panel a. The FWHM of the resonance peak in each STS spectrum is extracted from the Gaussian fitting. (d) The relation between the FWHM of the resonance peak and the width of the ABC-TG in tMBG.

platform for realizing one-dimensional superlattice potential for electrons.

Local stacking orders in the tMBG after the atomic reconstruction, which host quite different electronic structures, can be easily distinguished by means of STM and STS measurements. Figure 2(a) shows a representative STM image of a tiny-angle tMBG under a slight heterostrain. As we can see, there are three regions with distinct contrasts, which are naturally relative to the ABB, ABA, and ABC stacking configurations. The corresponding STS spectra acquired at the center of each stacking configuration are given in Fig. 2(b). Firstly, we can identify the ABB stacked region from the STM image directly, since it is energetically unfavorable and prefers to shrink into a small dot. Then, the alternatively arranged ABA and ABC stacked regions can be distinguished as dark and bright STM contrasts with the combination of STM and STS measurements for the following reasons. On the one hand, the low-energy band structures of the ABA stacked trilayer graphene are composed of both the monolayer- and bilayer-graphene-like bands, which are supposed to exhibit a V-shaped spectrum [green line in Fig. 2(b)], as previously reported [53,54]. On the other hand, the ABC-TG band structures host a pair of cubic bands touching near the Fermi energy [55,56], thus generating a pronounced low-energy peak [yellow line in Fig. 2(b)].

The ABA and ABC stacking orders in the tMBG can also be clearly visualized from the spatially resolved charge distribution. As representatively shown in Figs. 2(c)–2(e), the STS maps acquired at the same location of Fig. 2(a) under different electron energies exhibit quite different electronic patterns. For example, the ABC-TG shows a much brighter contrast under −24 and 30 meV while a darker contrast at 256 meV in the STS maps, which are consistent with the different spectrum weight between the ABA and ABC stacking orders. More importantly, within each stacking configuration, the contrast in STS maps for all the energies are almost the same, implying the local atomic arrangement is quite homogeneous. Therefore, our results unambiguously demonstrate the realization of large-area and periodic ABC-TG regions constructed by the tMBG after the atomic reconstruction.

Now we turn to examine the stability of the ABC-TG constructed by the tMBG. Our experiments indicate that the periodic ABC-TG regions are quite stable after thermal annealing up to about 300 °C and under traditional STM measurements, which implies that the ABC-TG region is stabilized by the moiré structure of the tMBG. To further explore

the stability of the obtained ABC-TG regions, we apply a large STM tip pulse onto the tMBG with a pulse voltage of 6 V for 60 ms, which locally changes the moiré structure in the tMBG. The evolution of the stacking orders of the tMBG can be recorded by continuously measuring the STM topography images at the same location, as summarized in Fig. 3 (for simplicity, the time of applying the tip pulse is set to 0). Obviously, there is an obvious transition between the ABC and ABA stacking orders around the tip-pulse position and the stacking orders become stable after 159 minutes of the tip pulse. Such a long-time relaxation can be attributed to the local heating effect and the electric field effect induced by the tip during the STM measurements, as reported previously [57,58]. Even with the local structural reconstruction in the tMBG, the ABC-TG regions always take up a certain proportion in the studied area. Comparing with the isolated ABC-TG constructed via exfoliation or CVD methods in previous studies [31,59], our ABC-TG confined in tiny-angle tMBG shows a significant advantage for the structural stability.

The ABC-TG regions in the tiny-angle tMBG provide an ideal platform to explore the finite size effect on the flat bands of the ABC-TG. Here we take the tMBG region shown in Fig. 4(a) as an example, where the size of the ABC-TG (enclosed by the yellow dotted lines) varies continuously. The width of the ABC-TG is defined as the lateral length marked by the black double-headed arrow in Fig. 4(a), and hence, the ABC-TG width has a spatial distribution from 0 to several hundreds of nanometers. It is worth noting that the STS spectra acquired on the ABC-TG with different widths exhibit pronounced differences, as typically shown in Fig. 3(b). To be specific, there is no peak feature in the STS spectrum acquired on the ABC-TG with the width of 8 nm, implying the absence of the flat bands. As the ABC-TG width increasing to 65 nm, a weak density-of-states (DOS) peak emerges near the Fermi energy, and such a peak is much more pronounced when the width reaches to 480 nm. Figure 4(c) shows the spatially resolved STS spectra in the ABC-TG region along the red arrow marked in Fig. 4(a), where the evolution of the low-energy DOS peak is guided by the dotted lines. Moreover, we extract the full width at half-maximum (FWHM) of the DOS peak via a Gaussian fitting, and then plot the FWHM as a function of the ABC-TG width, as summarized in Fig. 4(d). Remarkably, as the ABC-TG width increasing, the DOS peak emerges once the width reaches 64 nm, and gradually becomes narrower and higher until the width up to 100 nm. After that, the STS spectra are almost unchanged, exhibiting a quite similar behavior to that of pristine ABC-TLG as previously reported [41,53,60]. It is worth noting that the critical value of the ABC-TG width is of the same order as the Fermi wavelength, indicating that the formation of the flat band in ABC-TG may requires the width exceeding the Fermi wavelength. Similar observation has also been observed in different samples (see Fig. S4 [48]), which help us rule out any possible artifacts. Such a result implies a minimal size ∼100 nm for exploring emergent correlated physics in the ABC stacked graphene and indicates that the large-scale ABC-TG constructed by tMBG provides an unprecedented opportunity towards the flat-band engineering.

IV. CONCLUSIONS

In summary, we report a method to controllably fabricate the ABC-TG via a tMBG moiré engineering technique. Our ABC-TG samples can reach a sub–micrometer size and show significant advantages of stability. The STS measurements further reveal that the flat bands of the ABC-TG are very robust and exhibit the same bandwidth as the bulk phase when the size of ABC-TG is larger than about 100 nm. Taken together, our results, which greatly improve the success rate of realizing the ABC-TG, highlight the tiny-angle tMBG to be a promising platform for exploring emergent physics in strongly correlated regimes.

ACKNOWLEDGMENTS

This work was supported by the National Key R&D Program of China (Grants No. 2022YFA1402502, No. 2021YFA1401900, No. 2021YFA1400100, and No. 2022YFA1402602), National Natural Science Foundation of China (Grants No. 12141401 and No. 12274026), "the Fundamental Research Funds for the Central Universities" and the China Postdoctoral Science Foundation (2023M740296).

[1] Y. Cao, V. Fatemi, A. Demir, S. Fang, S. L. Tomarken, J. Y. Luo, J. D. Sanchez-Yamagishi, K. Watanabe, T. Taniguchi, E. Kaxiras, R. C. Ashoori, and P. Jarillo-Herrero, Correlated insulator behaviour at half-filling in magic-angle graphene superlattices, Nature (London) **556**, 80 (2018).

[2] Y. Xie, B. Lian, B. Jäck, X. Liu, C.-L. Chiu, K. Watanabe, T. Taniguchi, B. A. Bernevig, and A. Yazdani, Spectroscopic signatures of many-body correlations in magic-angle twisted bilayer graphene, Nature (London) **572**, 101 (2019).

[3] Z. Hao, A. M. Zimmerman, P. Ledwith, E. Khalaf, D. H. Najafabadi, K. Watanabe, T. Taniguchi, A. Vishwanath, and P. Kim, Electric field–tunable superconductivity in alternating-twist magic-angle trilayer graphene, Science **371**, 1133 (2021).

[4] H. Kim, Y. Choi, C. Lewandowski, A. Thomson, Y. Zhang, R. Polski, K. Watanabe, T. Taniguchi, J. Alicea, and S. Nadj-Perge, Evidence for unconventional superconductivity in twisted trilayer graphene, Nature (London) **606**, 494 (2022).

[5] X. Liu, N. J. Zhang, K. Watanabe, T. Taniguchi, and J. I. A. Li, Isospin order in superconducting magic-angle twisted trilayer graphene, Nat. Phys. **18**, 522 (2022).

[6] A. Fischer, Z. A. H. Goodwin, A. A. Mostofi, J. Lischner, D. M. Kennes, and L. Klebl, Unconventional superconductivity in magic-angle twisted trilayer graphene, npj Quantum Mater. **7**, 5 (2022).

[7] G. W. Burg, J. Zhu, T. Taniguchi, K. Watanabe, A. H. MacDonald, and E. Tutuc, Correlated insulating states in twisted double bilayer graphene, Phys. Rev. Lett. **123**, 197702 (2019).

[8] C. Rubio-Verdú, S. Turkel, Y. Song, L. Klebl, R. Samajdar, M.-S. Scheurer, J.-W. Venderbos, K. Watanabe, T. Taniguchi,

H. Ochoa, L. Xian, D.-M. Kennes, R.-M. Fernandes, and A. N. Pasupathy, Moiré nematic phase in twisted double bilayer graphene, Nat. Phys. **18**, 196 (2022).

[9] C. Shen, Y. Chu, Q. Wu, N. Li, S. Wang, Y. Zhao, J. Liu J.Tang, J. Tian, K. Watanabe, T. Taniguchi, R. Yang, Z. Meng, D. Shi, O. V. Yazyev, and G. Zhang, Correlated states in twisted double bilayer graphene, Nat. Phys. **16**, 520 (2020).

[10] M. He, Y. Li, J. Cai, Y. Liu, K. Watanabe, T. Taniguchi, X. Xu, and M. Yankowitz, Symmetry breaking in twisted double bilayer graphene, Nat. Phys. **17**, 26 (2021).

[11] A. L. Sharpe, E. J. Fox, A. W. Barnard, J. Finney, K. Watanabe, T. Taniguchi, M. A. Kastner, and D. Goldhaber-Gordon, Emergent ferromagnetism near three-quarters filling in twisted bilayer graphene, Science **365**, 605 (2019).

[12] X. Liu, Z. Hao, E. Khalaf, J. Y. Lee, Y. Ronen, H. Yoo, H. D., K. Watanabe Najafabadi, T. Taniguchi, A. Vishwanath, and P. Kim, Tunable spin-polarized correlated states in twisted double bilayer graphene, Nature (London) **583**, 221 (2020).

[13] Z. Zhang, E. C. Regan, D. Wang, W. Zhao, S. Wang, M. Sayyad, K. Yumigeta, K. Watanabe, T. Taniguchi, S. Tongay, M. Crommie, A. Zettl, M. P. Zaletel, and F. Wang, Correlated interlayer exciton insulator in heterostructures of monolayer WSe_2 and moiré WS_2/WSe_2, Nat. Phys. **18**, 1214 (2022).

[14] P. Wang, G. Yu, Y. H. Kwan, Y. Jia, S. Lei, S. Klemenz, F. A. Cevallos, R. Singha, T. Devakul, K. Watanate, T. Taniguchi, S. Sondhi, R. J. Cava, L. M. Schoop, S. A. Parameswaran, and S. Wu, One-dimensional Luttinger liquids in a two-dimensional moiré lattice, Nature (London) **605**, 57 (2022).

[15] E. C. Regan, D. Wang, C. Jin, M. I. Utama, B. Gao, X. Wei, S. Zhao, W. Zhao, Z. Zhang, K. Yumigeta, M. Blei, J. D. Carlström, K. Watanabe, T. Taniguchi, S. Tongay, M. Crommie, A. Zettl, and F. Wang, Mott and generalized Wigner crystal states in WSe_2/WS_2 moiré superlattices, Nature (London) **579**, 359 (2020).

[16] X. Huang, T. Wang, S. Miao, C. Wang, Z. Li, Z. Lian, K. Watanabe T.Taniguchi, S. Okamoto, D. Xiao, S.-F. Shi, and Y.-T. Cui, Correlated insulating states at fractional fillings of the WS_2/WSe_2 moiré lattice, Nat. Phys. **17**, 715 (2021).

[17] H. Li, S. Li, E. C. Regan, D. Wang, W. Zhao, S. Kahn, K. Yumigeta, M. Blei, T. Taniguchi, K. Watanabe, S. Tongay, A. Zettl, M. F. Crommie, and F. Wang, Imaging two-dimensional generalized Wigner crystals, Nature (London) **597**, 650 (2021).

[18] G. Chen, A. L. Sharpe, E. J. Fox, Y.-H. Zhang, S. Wang, L. Jiang, B. Lyu, H. Li, K. Watanabe, T. Taniguchi, Z. Shi, T. Senthil, D. Goldhaber-Gordon, Y. Zhang, and F. Wang, Tunable correlated Chern insulator and ferromagnetism in a moiré superlattice, Nature (London) **579**, 56 (2020).

[19] J.-X. Lin, Y.-H. Zhang, E. Morissette, Z. Wang, S. Liu, D. Rhodes, K. Watanabe, T. Taniguchi, J. Hone, and J. I. A. Li, Spin-orbit-driven ferromagnetism at half moiré filling in magic-angle twisted bilayer graphene, Science **375**, 437 (2022).

[20] S. Lisi, X. Lu, T. Benschop, T. A. Jong, P. Stepanov, J. R. Duran, F. Margot, I. Cucchi, E. Cappelli, A. Hunter, A. Tamai, V. Kandyba, A. Giampietri, A. Barnov, J. Jobst, V. Stalman, M. Leeuwenhoek, K. Watanabe, T. Taniguchi, L. Rademaker, S. J. Molen, M. P. Allan, D. K. Efetov, and F. Baumbeiger, Observation of flat bands in twisted bilayer graphene, Nat. Phys. **17**, 189 (2021).

[21] M. Christos, S. Sachdev, and M. S. Scheurer, Correlated insulators, semimetals, and superconductivity in twisted trilayer graphene, Phys. Rev. X **12**, 021018 (2022).

[22] M. H. Naik and M. Jain, Ultraflatbands and shear solitons in moiré patterns of twisted bilayer transition metal dichalcogenides, Phys. Rev. Lett. **121**, 266401 (2018).

[23] F. Wu, T. Lovorn, E. Tutuc, and A. H. MacDonald, Hubbard model physics in transition metal dichalcogenide moiré bands, Phys. Rev. Lett. **121**, 026402 (2018).

[24] N. N. T. Nam and M. Koshino, Lattice relaxation and energy band modulation in twisted bilayer graphene, Phys. Rev. B **96**, 075311 (2017).

[25] I. Hagymási, M. S. Mohdisa, Z. Tajkov, K. Marity, L. Oroszlány, J. Koltai, A. Alassaf, P. Kun, K. Kandrai, A. Pálinkás, P. Vancsó, L. Tapasztp, and P. Nemes-Incze, Observation of competing, correlated ground states in the flat band of rhombohedral graphite, Sci. Adv. **8**, eabo6879 (2022).

[26] T. Han, Z. Lu, G. Scuri, J. Sung, J. Wang, T. Han, K. Watanabe, L. Fu T.Taniguchi, H. Park, and L. Ju, Orbital multiferroicity in pentalayer rhombohedral graphene, Nature (London) **623**, 41 (2023).

[27] H. Zhou, T. Xie, A. Ghazaryan, T. Holder, J. R. Ehrets, E. M. Spanton, T. Taniguchi, K. Watanabe, E. Berg, M. Serbyn, and A. F. Young, Half- and quarter-metals in rhombohedral trilayer graphene, Nature (London) **598**, 429 (2021).

[28] A. Kerelsky, C. Rubio-Verdú, L. Xian, and A. N. Pasupathy, Moiréless correlations in ABCA graphene, Proc. Natl. Acad. Sci. USA **118**, e2017366118 (2021).

[29] D. Xiao, M.-C. Chang, and Q. Niu, Berry phase effects on electronic properties, Rev. Mod. Phys. **82**, 1959 (2010).

[30] R. R. Haering, Band structure of rhombohedral graphite, Can. J. Phys. **36**, 3 (1958).

[31] G. Chen, L. Jiang, S. Wu, B. Lyu, H. Li, B. L. Chittari, K. Watanabe, T. Taniguchi, Z. Shi, J. Jung, Y. Zhang, and F. Wang, Evidence of a gate-tunable mott insulator in a trilayer graphene moiré superlattice, Nat. Phys. **15**, 237 (2019).

[32] G. Chen, A. L. Sharpe, P. Gallagher, I. T. Rosen, E. J. Fox, L. Jiang, B. Lyu, H. Li, K. Watanabe, T. Taniguchi, J. Jung, Z. Shi, D. Goldhaber-Gordon, Y. Zhang, and F. Wang, Signatures of tunable superconductivity in a trilayer graphene moiré superlattice, Nature (London) **572**, 215 (2019).

[33] G. Chen, A. L. Sharpe, E. J. Fox, S. Wang, B. Lyu, L. Jiang, H. Li, K. Watanabe, T. Taniguchi, M. F. Crommie, M. A. Kastner, Z. Shi, D. Goldhaber-Gordon, Y. Zhang, and F. Wang, Tunable orbital ferromagnetism at noninteger filling of a moiré superlattice, Nano Lett. **22**, 238 (2022).

[34] K. Liu, J. Zheng, Y. Sha, B. Lyu, F. Li, Y. Park, Y. Ren, K. Watanabe, T. Taniguchi, J. Jia, W. Luo, Z. Shi, J. Jung, and G. Chen, Spontaneous broken-symmetry insulator and metals in tetralayer rhombohedral graphene, Nat. Nanotechnol. **19**, 188 (2023).

[35] F. Zhang, J. Jung, G. A. Fiete, Q. Niu, and A. H. MacDonald, Spontaneous quantum Hall states in chirally stacked few-layer graphene systems, Phys. Rev. Lett. **106**, 156801 (2011).

[36] J. Dong, T. Wang, T. Wang, T. Soejima, M. P. Zaletel, A. Vishwanath, and D. E. Parker, Anomalous Hall crystals in rhombohedral multilayer graphene I: Interaction-driven Chern bands and fractional quantum Hall states at zero magnetic field, arXiv:2311.05568.

[37] Z. Dong, A. S. Patri, and T. Senthil, Theory of fractional quantum anomalous Hall phases in pentalayer rhombohedral graphene moiré structures, arXiv:2311.03445.

[38] T. Han, Z. Lu, G. Scuri, J. Sung, J. Wang, T. Han, K. Watanabe, T. Taniguchi, H. Park, and L. Ju, Correlated insulator and Chern insulators in pentalayer rhombohedral-stacked graphene, Nat. Nanotechnol. **19**, 181 (2023).

[39] J. Herzog-Arbeitman, Y. Wang, J. Liu, P. M. Tam, Z. Qi, Y. Jia, D. K. Efetov, O. Vafek, N. Regnauil, H. Wang, Q. Wu, B. A. Bernevig, and J. Yu, Moiré fractional Chern insulators II: First-principles calculations and continuum models of rhombohedral graphene superlattices, Phys. Rev. B **109**, 205122 (2024).

[40] Z. Lu, T. Han, Y. Yao, A. P. Reddy, J. Yang, J. Seo, K. Watanabe, T. Taniguchi, L. Fu, and Ju L, Fractional quantum anomalous Hall effect in multilayer graphene, Nature (London) **626**, 759 (2024).

[41] C. H. Lui, Z. Li, K. F. Mak, E. Cappelluti, and T. F. Heinz, Observation of an electrically tunable band gap in trilayer graphene, Nat. Phys. **7**, 944 (2011).

[42] C. H. Lui, Z. Li, Z. Chen, P. V. Klimov, L. E. Brus, and T. F. Heinz, Imaging stacking order in few-layer graphene, Nano Lett. **11**, 164 (2011).

[43] W. Zhang, J. Yan, C.-H. Chen, L. Lei, J.-L. Kuo, Z. Shen, and L.-J. Li, Molecular adsorption induces the transformation of rhombohedral- to Bernal-stacking order in trilayer graphene, Nat. Commun. **4**, 2074 (2013).

[44] Z. Gao, S. Wang, J. Berry, Q. Zhang, J. Gebhardt, W. M. Parkin, J. Avila, H. Yi, C. Chen, S. Hurtado-parra, M. Drndic, A. M. Rappe, D. J. Srolovitz, J. M. Kikkawa, Z. Luo, M.C. Asensio, F. Wang, and A. T. Johnson, Large-area epitaxial growth of curvature-stabilized ABC trilayer graphene, Nat. Commun. **11**, 546 (2020).

[45] K. Kim, M. Yankowitz, B. Fallahazad, S. Kang, H. C. P. Movva, S. Huang, S. Larentis, C. M. Corbet, T. Taniguchi, K. Watenabe, S. K. Banerjee, B. J. Leroy, and E. Tutuc, van der Waals heterostructures with high accuracy rotational alignment, Nano Lett. **16**, 1989 (2016).

[46] F. Pizzocchero, L. Gammelgaard, B. S. Jessen, J. M. Caridad, L. Wang, J. Hone, P. Boggild, and T. J. Booth, The hot pick-up technique for batch assembly of van der Waals heterostructures, Nat. Commun. **7**, 11894 (2016).

[47] D. G. Purdie, N. M. Pugno, T. Taniguchi, K. Watanabe, A. C. Ferrari, and A. Lombardo, Cleaning interfaces in layered materials heterostructures, Nat. Commun. **9**, 5387 (2018).

[48] See Supplemental Material at http://link.aps.org/supplemental/10.1103/PhysRevB.109.205155 for the detailed sample preparation and STM/STS measurements,

[49] H. Polshyn, J. Zhu, M. A. Kumar, Y. Zhang, F. Yang, C. L. Tschirhart, K. Watanabe M.Serlin, T. Taniguchi. A. H. MacDonald, and A. F. Young, Electrical switching of magnetic order in an orbital Chern insulator, Nature (London) **588**, 66 (2020).

[50] S. Xu, M. M. Ezzi, N. Balakrishnan, A. Garcia-Ruiz, B. Tsim, C. Mullan, J. Barrier, B. A. Piot N.Xin, T. Taniguchi, K. Watanabe, A. Carvalho, A. Mishchenko, A. K. Geim, V. I. Faĺko, S. Adam, A. H. Castro Neto, K. S. Novoselov, and Y. Shi, Tunable van Hove singularities and correlated states in twisted monolayer-bilayer graphene, Nat. Phys. **17**, 619 (2021).

[51] X.-F. Zhou, Y.-W. Liu, C.-Y. Hao, C. Yan, Q. Zheng, Y.-N. Ren, Y.-X. Zhao, K. Watanabe, T. Taniguchi, and L. He, Coexistence of reconstructed and unreconstructed structures in the structural transition regime of twisted bilayer graphene, Phys. Rev. B **107**, 125410 (2023).

[52] Y.-W. Liu, Y. Su, X.-F. Zhou, L. J. Yin, C. Yan, S.-L. Li, W. Yan, S. Han, Z.-Q. Fu, Y. Zhang, Q. Yang, Y.-N. Ren, and L. He, Tunable lattice reconstruction, triangular network of chiral one-dimensional states, and bandwidth of flat bands in magic angle twisted bilayer graphene, Phys. Rev. Lett. **125**, 236102 (2020).

[53] L.-J. Yin, W.-X. Wang, Y. Zhang, Y.-Y. Ou, H.-T. Zhang, C.-Y. Shen, and L. He, Observation of chirality transition of quasiparticles at stacking solitons in trilayer graphene, Phys. Rev. B **95**, 081402(R) (2017).

[54] L.-J. Yin, L.-J. Shi, S.-Y. Li, Y. Zhang, Z.-H. Guo, and L. He, High-magnetic-field tunneling spectra of *ABC*-stacked trilayer graphene on graphite, Phys. Rev. Lett. **122**, 146802 (2019).

[55] L. Zhang, Y. Zhang, J. Camacho, M. Khodas, and I. Zaliznyak, The Experimental observation of quantum Hall effect of L = 3 chiral quasiparticles in trilayer graphene, Nat. Phys. **7**, 953 (2011).

[56] F. Zhang, B. Sahu, H. Min, and A. H. MacDonald, Band structure of *ABC*-stacked graphene trilayers, Phys. Rev. B **82**, 035409 (2010).

[57] Y. Zhao, X. Zhou, Y. Zhang, and L. He, Oscillations of the spacing between van Hove singularities induced by sub-ångstrom fluctuations of interlayer spacing in graphene superlattices, Phys. Rev. Lett. **127**, 266801 (2021).

[58] P. Xu, M. Neek-Amal, S. D. Barber, J. K. Schoelz, M. L. Ackerman, P. M. Thibado, A. Sadeghi, and F. M. Peeters, Unusual ultra-low-frequency fluctuations in freestanding graphene, Nat. Commun. **5**, 3720 (2014).

[59] M. Yankowitz, J. I.-J. Wang, A. G. Birdwell, Y.-A. Chen, K. Watanabe, T. Taniguchi, P. Jacquod, P. San-Jose, P. Jarillo-Herrero, and B. J. LeRoy, Electric field control of soliton motion and stacking in trilayer graphene, Nat. Mater. **13**, 786 (2014).

[60] L.-J. Yin, S.-Y. Li, J.-B. Qiao, J.-C. Nie, and L. He, Landau quantization in graphene monolayer, Bernal bilayer, and Bernal trilayer on graphite surface, Phys. Rev. B **91**, 115405 (2015).